Subseasonal Variations of Rainfall in South America in the Vicinity of the Low-Level Jet East of the Andes and Comparison to Those in the South Atlantic Convergence Zone

BRANT LIEBMANN

NOAA–CIRES Climate Diagnostics Center, Boulder, Colorado

GEORGE N. KILADIS

NOAA Aeronomy Laboratory, Boulder, Colorado

CAROLINA S. VERA AND A. CELESTE SAULO

Centro de Investigaciones del Mar y la Atmósfera/CONICET, Departamento de Ciencias de la Atmósfera y los Océanos, Universidad de Buenos Aires, Buenos Aires, Argentina

LEILA M. V. CARVALHO

Department of Atmospheric Sciences, Institute of Astronomy, Geophysics and Atmospheric Sciences, University of São Paulo, São Paulo, Brazil

(Manuscript received 16 January 2003, in final form 20 February 2004)

ABSTRACT

Regional and large-scale circulation anomalies associated with variations in rainfall downstream of the South American low-level jet are identified and compared to those in the South Atlantic convergence zone (SACZ). Composites of precipitation associated with strong jets reveal an approximate doubling of the quantities one would expect from climatology, with an evolution of the rainfall pattern from south to north. The occurrence of extreme precipitation events follows a similar pattern. Meridional cross sections of composite wind reveal a distinct low-level jet near 20°S and a baroclinic development farther south that appears to force the jet. Geopotential height, temperature, and large-scale wind composites suggest that this developing disturbance is tied to a wave train that originates in the midlatitude Pacific and turns equatorward as it crosses the Andes Mountains. Similar composites based on SACZ rainfall reveal similar features, but of opposite sign, suggesting that the phase of the wave as it crosses the Andes Mountains determines whether rainfall will be enhanced downstream of the jet or in the SACZ. The alternate suppression or enhancement of rainfall in these adjacent regions results in a precipitation ''dipole.'' Many previous studies have found a similar out-of-phase relationship over many time scales. The phase of the Madden–Julian oscillation (MJO) is composited relative to anomalous precipitation events, revealing statistically relevant amplitudes associated with rainfall both downstream of the jet and in the SACZ. The MJO is a particularly interesting intraseasonal oscillation because it has some predictability. It is speculated that the slowly varying dipole that has been observed is a consequence of the preferred phasing of synoptic waves due to variations of the planetary-scale basic-state flow, which is at times associated with the MJO.

1. Introduction

A low-level jet (LLJ) stream occurs frequently to the east of the Andes Mountains of South America in all seasons (e.g., Stensrud 1996; Douglas et al. 2000; Paegle 2000; Douglas et al. 1998; Marengo et al. 2002). This feature is thought to be responsible for transporting large quantities of water vapor into central and southern South America (e.g., Berri and Inzunza 1993; Mo and Higgins 1996; Nogués-Paegle and Mo 1997; Li and Le Treut 1999; Saulo and Nicolini 2000; Silva Dias 2000; Salio et al. 2002). Although the original definition of LLJ is related to the mesoscale characteristics of the low-level flow (Bonner 1968), this name has been extended to identify, from a large-scale perspective, the moisture corridor that exists along the eastern slope of the Andes resulting from the split of the trade winds upon approaching the mountains (Silva Dias 2000). Variations of the jet are related to synoptic activity (e.g.,

Corresponding author address: Dr. Brant Liebmann, NOAA–CIRES Climate Diagnostics Center, R/CDC1, 325 Broadway, Boulder, CO 80305-3328.
E-mail: Brant.Liebmann@noaa.gov

Douglas et al. 1998, 2000; Saulo and Nicolini 2000; Vera et al. 2002), although the jet would likely exist in the absence of synoptic forcing because of interaction between mean westerly flow and the Andes (Campetella and Vera 2002) and because of heating on a sloping terrain (e.g., Stensrud 1996). The position of the jet, its strength, and its diurnal cycle may be substantially altered by the impact of latent heating in the central Brazilian Amazon basin (Silva Dias 2000).

The LLJ is of more than academic interest because the La Plata River basin of central South America, the likely depository for the flux of water vapor associated with the jet, is approximately the same size as the Mississippi River basin of North America. The basin drains parts of five countries, contains half of their combined population, and produces 70% of their combined gross national products, much of it agricultural.

Another major climatological feature of South America during summer is the South Atlantic convergence zone (SACZ). The SACZ is a band of enhanced cloudiness and precipitation that extends southeastward from the Amazon basin into the Atlantic (e.g., Kodama 1993; Figueroa et al. 1995; Casarin and Kousky 1986; Nogués-Paegle and Mo 1997; Lenters and Cook 1999; Liebmann et al. 1999), passing over major population centers of Brazil. The most coherent forcing of the SACZ appears to be synoptic-scale waves from the midlatitudes (e.g., Sugahara et al. 1994; Liebmann et al. 1999), but forcing of the large-scale flow by Amazon convection is likely important in maintaining its mean position (e.g., Figueroa et al. 1995).

There is mounting evidence that when moisture flux into central South America via the low-level jet is strong, SACZ convection is weak, and vice versa. Using a rotated empirical orthogonal function (EOF) analysis of 10–90-day bandpassed outgoing longwave radiation (OLR), Nogués-Paegle and Mo (1997) found an ''oscillation'' with a half period of about 10 days, which they referred to as the South American seesaw pattern. A similar result was obtained by Liebmann et al. (1999) when they regressed OLR in the vicinity of the SACZ onto the OLR field, although they used 2–30-day filtered data and estimated a period of about 13 days. Herdies et al. (2002) constructed composites based on the direction of the low-level zonal wind near 11°S, 62°W during January and February 1999. They found that westerly winds were associated with an active SACZ and net moisture divergence over southwestern Brazil, northern Argentina, and Paraguay (implying a weak LLJ), while easterly winds were associated with moisture convergence and a weak SACZ. Jones and Carvalho (2002), using 10–70-day filtered data at the same point, also found westerlies to be associated with enhanced rainfall in the vicinity of the SACZ.

The aforementioned papers concentrated on the intraseasonal signal of the precipitation (or precipitation proxy) variability. Thus far, there have been few studies of whether the seesaw pattern also modulates the occurrence of heavy precipitation events. Moreover, there is no evidence in the literature regarding the possible relationship between the LLJ and extreme precipitation events over subtropical South America. Therefore, precipitation anomalies and those of heavy daily rainfall events will be documented in association with strong LLJ episodes during austral summer. Then the synoptic patterns associated with rain events in the vicinity of the jet will be compared to synoptic patterns in the context of rainfall in the SACZ, and vice versa. Previous works have shown that these patterns are out of phase, although an explanation of this behavior is lacking.

It has also been recognized that the activity of intraseasonal oscillations has an impact over South America. Regressing 30–70-day bandpassed OLR against upper-level winds, Kiladis and Weickmann (1992) showed a signal south of the mean SACZ position following an OLR anomaly over the equatorial western Pacific. Paegle et al. (2000) found that the South American seesaw pattern is influenced by oscillatory modes with periods both of 22–28 and 36–40 days. Furthermore, Marton and Silva Dias (2001) show that other oscillations with distinct periods between 10 and 70 days also play a significant role in South American precipitation. Thus far, however, the 30–60-day band, which is related to the Madden–Julian oscillation (MJO; Madden and Julian 1994), is the only one whose potential predictability has been demonstrated (e.g., Ferranti et al. 1990; Jones et al. 2004). In fact, the MJO is currently being operationally monitored and used as a predictor for experimental forecasts (K. Weickmann 2002, personal communication). Therefore, the focus of this paper is to explore the relationship between rainfall, the LLJ, the SACZ, and the MJO.

2. Data

Daily rainfall accumulations from more than 1500 stations are used to obtain the patterns of rainfall shown below (for sources see the acknowledgments). These data extend from 1976 to 2000. The highest density of stations is in Brazil. The following analyses involving individual stations require at least 10 yr of data from each station with no more than 33% of days missing in years with data. On average, 14% of the data are considered missing in years with data. Some of our analysis involves data averaged onto a 2.5° grid. In this case, all stations with at least 4 yr of data and not more than 33% of those days missing are averaged into the value at the nearest grid point. OLR is also used as another measure of large-scale rainfall.

The circulation fields used in this study are from the National Centers for Environmental Prediction–National Center for Atmospheric Research reanalysis project (Kalnay et al. 1996) and are on a 2.5° grid. They are daily averages from 4-times-daily fields, beginning at 0000 UTC. Over South America, and especially in the vicinity of the LLJ, there are few upper-air observations,

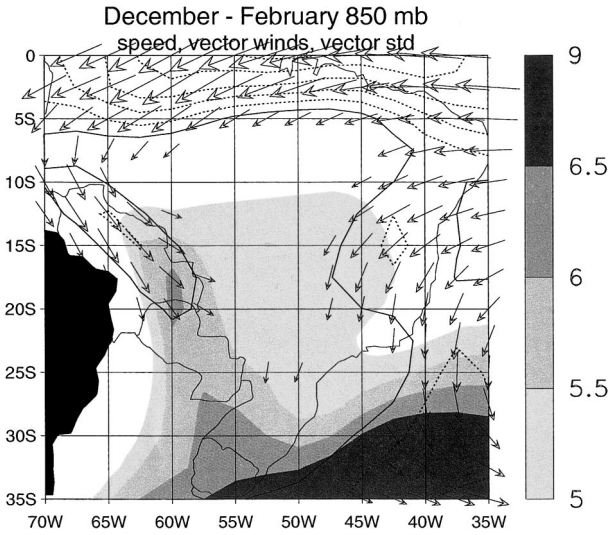

FIG. 1. DJF climatological 850-mb winds (vectors), speed (contoured), and vector standard deviation (shaded) for the period 1976–97. Vector plotting starts at 4 m s^{-1}. Contours start at 6 m s^{-1}, with an interval of 1.0 m s^{-1}. The 6 m s^{-1} contour is solid; the others are dotted. Areas with orography above 1400 m are shaded black.

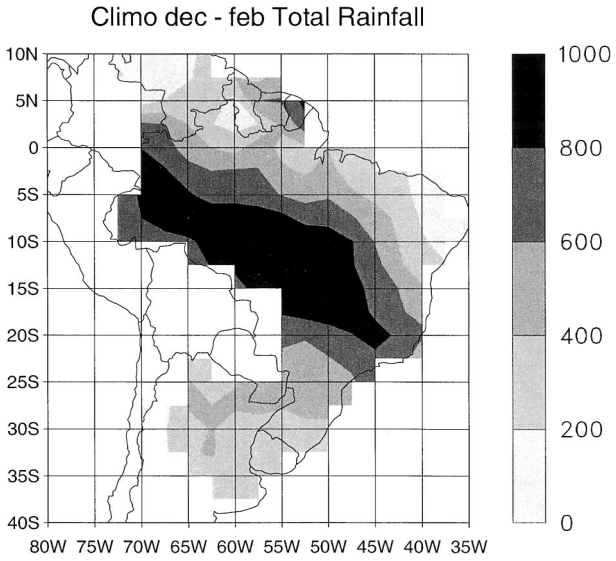

FIG. 2. Climatological DJF total rainfall (in mm) for the period 1976–97.

and thus the fields are quite model dependent. Most of the analyses shown below, however, were recalculated with reanalysis data from the European Centre for Medium-Range Weather Forecasts with nearly identical results.

In some datasets, rainfall is measured at 1200 UTC (the observation time for some datasets is unknown) and is recorded as the precipitation during the previous day. Thus there may be a slight discrepancy between the rain and meteorological fields, although this problem is considered to have only a minor impact on the applications discussed here.

3. Results

a. Climatology

1) IDENTIFICATION OF THE JET

The LLJ maximum in wind and water vapor transport have been identified to be at or below 850 mb along the east slope of the Andes using both gridded global analyses (e.g., Li and Le Treut 1999; Salio et al. 2002), direct observations (e.g., Douglas et al. 1998, 2000; Marengo et al. 2002), and regional model simulations (e.g., Berri and Inzunza 1993; Nicolini and Saulo 2000). Longitude–height cross sections from reanalyses (not shown) confirm a speed maximum near 850 mb in all seasons. The LLJ is most pronounced in summer, although Li and Le Treut (1999) found that mean southward moisture transport is actually larger during winter. This paper focuses on the summer [December–January–February (DJF)] season.

Figure 1 shows the DJF 850-mb average speed, vector wind field, and vector standard deviation of the daily winds. The amplitude of the vector standard deviation is defined as the square root of the sum of the variances of its components (Brooks and Carruthers 1953), which permits contributions from both changes in amplitude and phase. The strongest winds in the domain are the easterly trades along the equator. There is strong northeasterly flow over the easternmost part of the continent associated with the South Atlantic high and northwesterlies associated with the LLJ roughly paralleling the Andes. The maximum climatological wind speed associated with the jet is 7.1 m s^{-1} at 12.5°S, 65°W. The large variability of the subtropics extends northward into the exit region of the LLJ. The vector standard deviation of interannual winds (i.e., of seasonal averages over all years) is less than 10% of the daily standard deviation (which includes interannual variability) in the vicinity of the jet (not shown).

2) RAINFALL

The 1976–97 DJF rainfall climatology from gridded station data is shown in Fig. 2. Rainfall is maximum within a northwest–southeast band defining the SACZ, which continues off the coast into the southeast Atlantic. In areas with data, there is a fairly uniform decrease in rainfall from the maximum band into Paraguay and northern Argentina. Unfortunately, long records are unavailable in the area around the mean LLJ and its exit region.

b. Intraseasonal circulation and rainfall anomalies

1) RAINFALL ANOMALIES ASSOCIATED WITH THE JET

In both the jet core and location of maximum variability associated with the LLJ, the mean winds are

approximately northwesterly (Fig. 1). The amplitude of the standard deviation of the northwesterly component of wind (not shown) is more than 75% of that of the vector standard deviation near its maximum, and the fraction increases to the northwest. An index intended to capture the variability of the jet is calculated from the 850-mb northwesterly component at 20°S, 60°W. This grid point is near the southern edge of the jet speed maximum and within the region of maximum vector standard deviation (Fig. 1). There are only minor differences between the results presented below using this index and those obtained using an index of the meridional wind, which will not be shown.

The strongest jet events were identified as those days on which the northwesterly wind is at least one standard deviation above the DJF climatological mean. The cases determined by this criterion were compared to those determined by the jet definition proposed by Bonner (1968), in which jet events were considered to be those days with shear (defined as the speed at 850 mb minus the speed at 700 mb) larger than 6 m s^{-1}, subject to the additional constraint that the 850-mb speed was above 12 m s^{-1}. Most (66%) cases previously identified did not satisfy the Bonner criterion, although that was expected since the jet definition is applied here to daily averaged fields. The actual Bonner criterion is based on instantaneous fields, and it is more frequently satisfied at 0000 and 0600 UTC (Salio et al. 2002).

Figures 3a and 3b show composites of precipitation for days on which the jet is one standard deviation or more above and below the mean (16.7% and 16.5% of days). The null hypothesis is easily rejected for any shaded area (except those between ±2 mm) shown (assuming 1 degree of freedom for each excursion of the jet above or below the one standard deviation threshold).

When the jet is strong (Fig. 3a), an expected positive anomaly downstream of it is evident, consistent with the pattern produced by the Eta Model during the 1997/98 summer during times with a strong jet (Nicolini and Saulo 2000). There is a suggestion of the often-observed dipole between precipitation in this region and that in the SACZ. On the other hand, when the jet is weak (Fig. 3b), the dipole is of opposite sign and its anomalies are approximately equal. The result of a weak jet associated with enhanced rainfall in the SACZ is consistent with that obtained by Nieto Ferreira et al. (2003) when they computed the strength of the jet based on SACZ events.

Figure 4a shows the percent of rainfall that occurs one day before those 16.7% of days on which the jet is strongest. South of the index grid point, rainfall is approximately doubled compared to its expected amount. Over time, this signal amplifies and moves northeastward (Fig. 4b).

Heavy daily precipitation events are of particular interest because of their immediate and potentially dramatic impacts. Following Liebmann et al. (2001), extreme events are defined as occurring at each station when daily precipitation equals at least 10% of its DJF

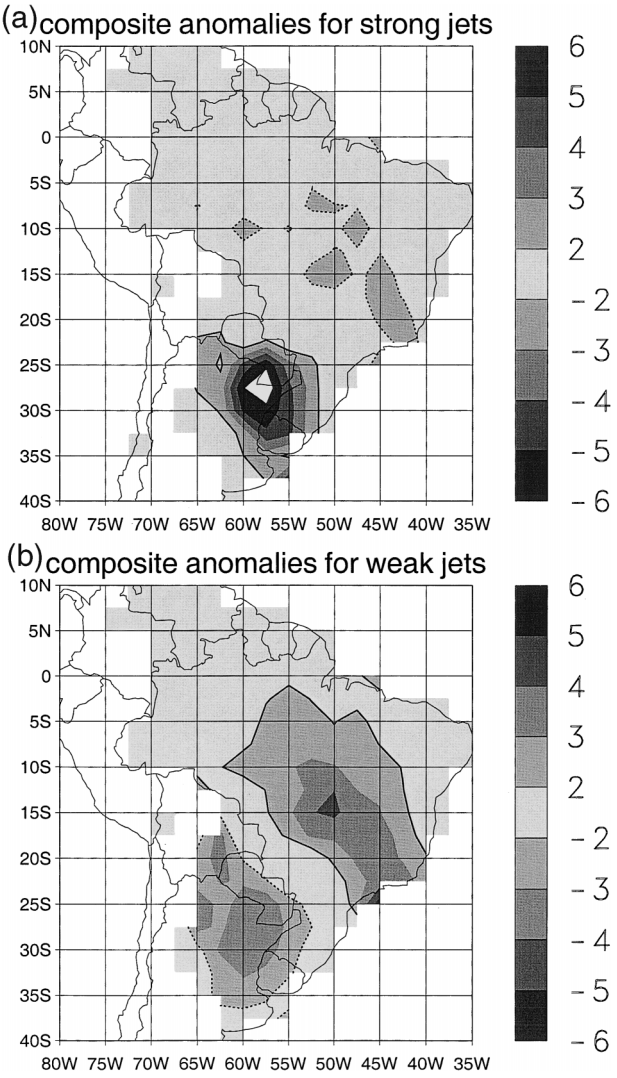

FIG. 3. Composite rainfall anomalies (from DJF climatology) for periods during which the northwesterly component of 850-mb wind at 20°S, 60°W is (a) above and (b) below 1 std dev of its DJF climatology. Solid (dotted) contour indicates the +2 (−2) mm day^{-1} anomaly.

climatological total. For the stations used in this study, rainfall was recorded on an average of 38.6 days during DJF. Thus, it is expected that 2.59% of the seasonal total will fall on a given rainy day. The percentage is about the same for stations south of 20°S. Here, the percent of extremes at each station associated with a strong jet is averaged onto a 2.5° grid. Using the same wind index as was used to produce Fig. 4, the percent of extreme events corresponding to strong jet cases is shown in Fig. 5a. South of the jet maximum, the pattern is similar to that of the total rainfall, although the percent of extreme events occurring on strong jet days approaches 50%, substantially higher than the percent of total rainfall in Fig. 4b. These results indicate a close correspondence between the strength of the LLJ and extreme rainfall

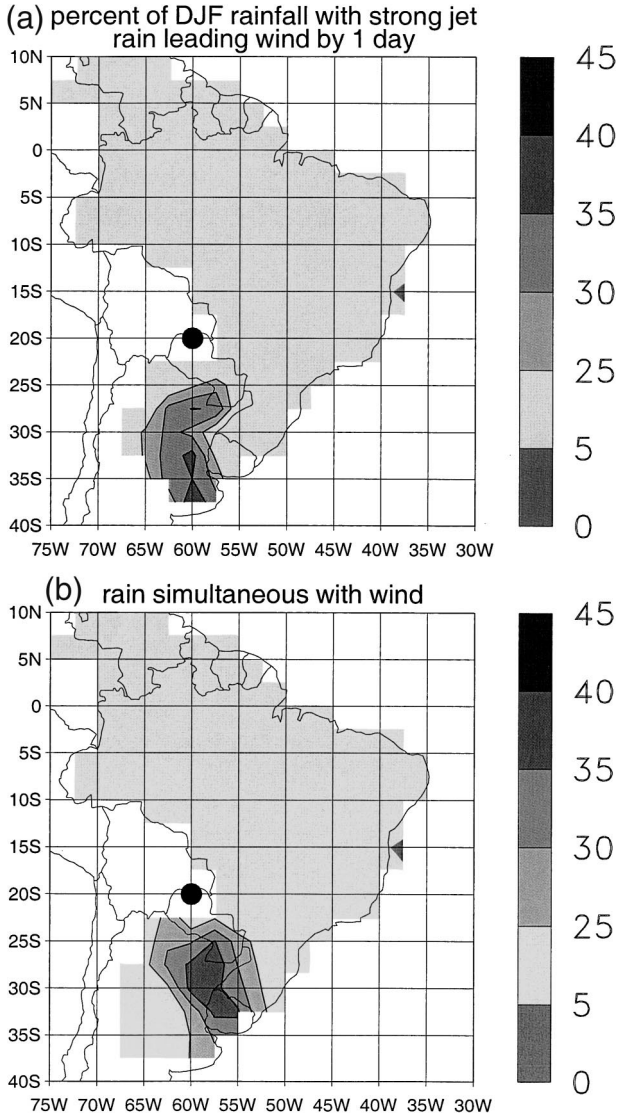

FIG. 4. Percent of total DJF rainfall for positive jet anomalies used to composite Fig. 3. Units are in percent of total rainfall during those periods, which make up 16.7% of all days. Contours begin at 25%, with an interval of 5%. (a) Rain 1 day prior to wind event. (b) Rain simultaneous with wind event.

anomalies to its south, in agreement with recent work that shows the close relationship between LLJ events and mesoscale convective systems responsible for heavy precipitation (Nieto Ferreira et al. 2003).

Straddling the equator in Fig. 5a is an interesting pattern of extreme event anomalies that is not mirrored on the total precipitation anomaly map. Throughout most of the near-equatorial Amazon basin south of the equator, extreme events are diminished. In northernmost South America, however, centered on Venezuela, extreme events are enhanced nearly to the same degree as to the south of the jet, although as it is the dry season there, the actual amount needed to qualify as an extreme event is substantially reduced compared to that during the summer season.

Figure 5b, which shows the percent of extreme events occurring on the 16.5% days during which the northwesterly component of the 850 mb at 20°S, 60°W is more than one standard deviation below its mean, is in marked contrast to the pattern of extremes during the strong jet cases shown in Fig. 5a. In this case, there are fewer-than-expected extremes downstream of the jet, and the only area with an increased occurrence of extremes is in a band centered slightly south of the SACZ.

2) CIRCULATION ASSOCIATED WITH RAINFALL ANOMALIES

A problem with using a location-dependent wind index as the key variable with which to examine the evolution of the circulation associated with strong jet episodes is that this will bias the result toward events at that location. The results of the previous section show that a substantial fraction of rainfall anomalies downstream of the LLJ are related to jet strength, as was found by Nicolini and Saulo (2000) using a broader definition of the jet that was not location dependent. Thus it seems reasonable to construct circulation composites using rainfall as the key variable, although this choice of variable does not completely eliminate the bias caused by using a fixed location.

Composites were produced by averaging those days on which rainfall at 30°S, 60°W (in the vicinity of the maximum rainfall anomaly associated with a strong jet as defined here) is at least one standard deviation above its DJF climatology. The composite longitude–pressure cross section of the meridional wind anomaly at 20°S is shown in Fig. 6a. A northerly anomaly of 4 m s^{-1} is centered at 60°W near 925 mb, with a low-level jet-like structure. The anomaly is also centered at the longitude of the climatological jet exit region, as is expected. At 30°S (Fig. 6b), however, the low-level jet is overshadowed by a westward tilting increase of wind with height, consistent with a baroclinic synoptic-scale system. A similar synoptic pattern is observed during winter, although during that season upper-level troughs crossing the continent provide a baroclinic environment north of 30°S where the LLJ is embedded (Vera et al. 2002).

The large-scale evolution of the 200- and 850-mb heights and winds associated with the events are shown in Figs. 7–10. These composites were made by identifying only the maximum anomaly during each excursion above one standard deviation. Two days prior to the rainfall event (Fig. 7), there is clear evidence of a wave train approaching South America from the west. As the upper-level height anomalies pass the Andes, they turn distinctly equatorward, following the preferred wave guiding induced by the basic state (Berbery et al. 1992; Ambrizzi and Hoskins 1997). There is some baroclinicity associated with this wave train, as seen by a slight westward tilt with height. At 850 mb, the low heights

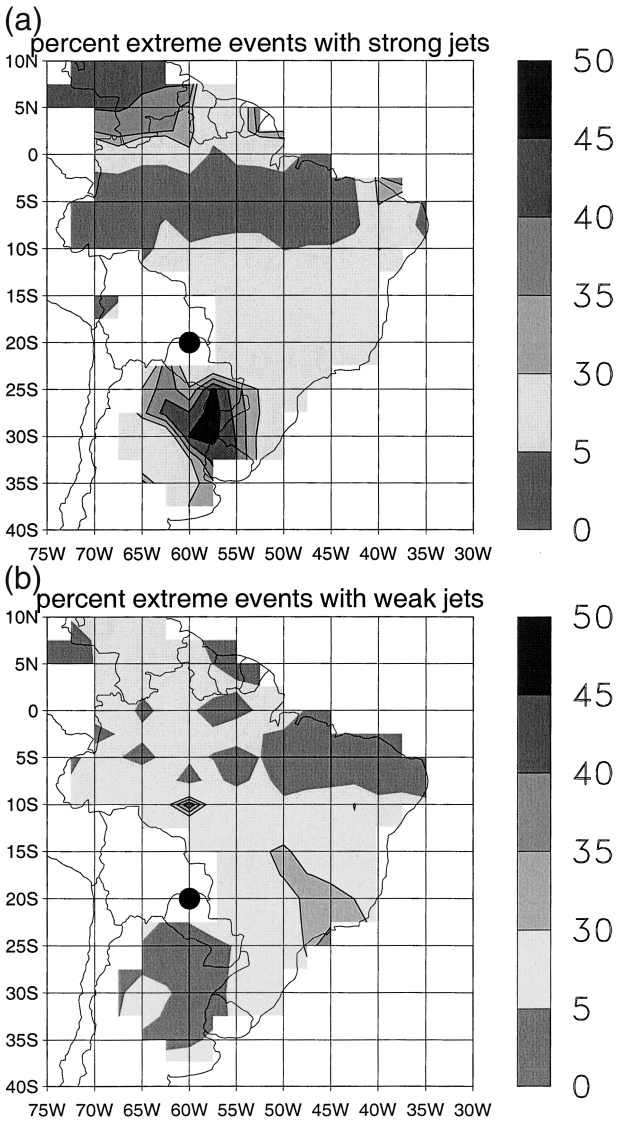

FIG. 5. (a) As in Fig. 4b, except quantity plotted is percent of extreme precipitation events, and contours begin at 30%. An extreme event is counted at each station when daily rainfall exceeds 10% of its DJF climatology, and is then averaged onto a 2.5° grid. (b) As in (a), except for 16.5% of days during which magnitude of northwesterly wind is 1 std dev below its mean.

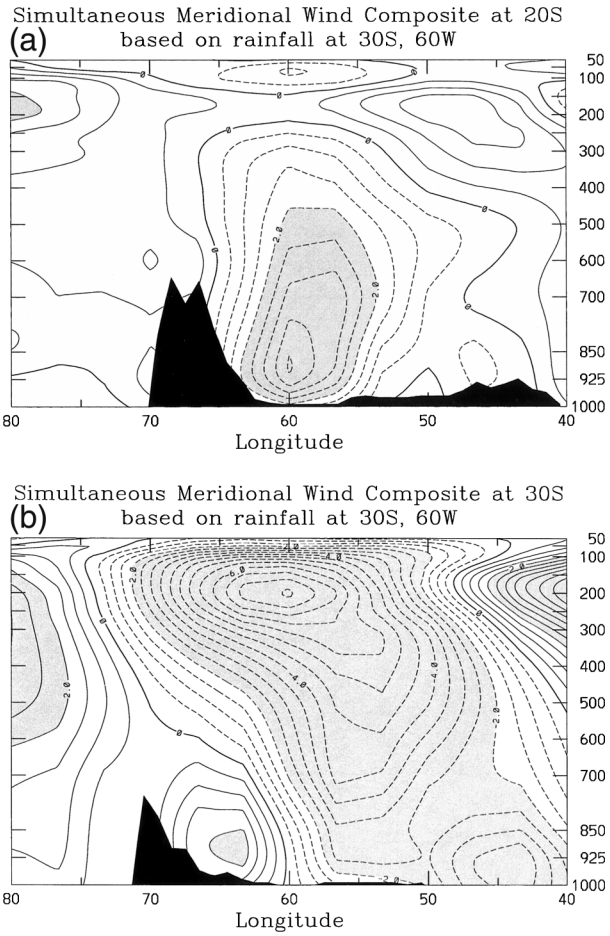

FIG. 6. (a) Simultaneous composite of meridional wind anomalies from DJF climatology along 20°S based on 1 std dev rain events at 30°S, 60°W. Units are in m s^{-1}, with an interval of 0.5 m s^{-1}, and negative contours are dashed. Dark shading indicates topography. (b) As in (a), except along 30°S.

have begun to move northward to the east of the Andes, consistent with a developing lee trough, but the center of the 850-mb circulation anomaly is farther to the south. Prior to this time (not shown), the upstream centers are higher in amplitude and slightly to the west compared to those shown in Fig. 7.

One day later, a day before the rain event (Fig. 8), the upper-level centers over the continent continue to develop while the upstream centers begin to weaken. The low-level centers, however, weaken, except for the equatorward extension of the low near the rain index point. Vera et al. (2002) showed that such low-level cyclone weakening is associated with changes in its baroclinic structure exerted by the presence of the Andes. This is the time of maximum strength of the LLJ.

On the day of the rain event (Fig. 9), the upper-level downstream high continues to develop. At lower levels, a weak negative height anomaly is observed at subtropical latitudes just east of the Andes. The associated wind anomalies exhibit an abrupt shift in the southwest to northeast direction, which is typically indicative of a frontal zone over this region during summer (Garreaud and Wallace 1998), as the midlatitude cyclone center moves rapidly eastward. A day after the rain event (Fig. 10), the upper-level pattern continues to propagate slowly eastward, but the 850-mb winds have weakened over the continent, and the low-level cyclone and associated frontal zone is now over the ocean. In fact, the low center has intensified such that, in contrast to the upper level, the pattern is quite zonal.

It is interesting to compare the patterns associated with rainfall in the vicinity of the low-level jet with those in the SACZ. SACZ rainfall will be considered

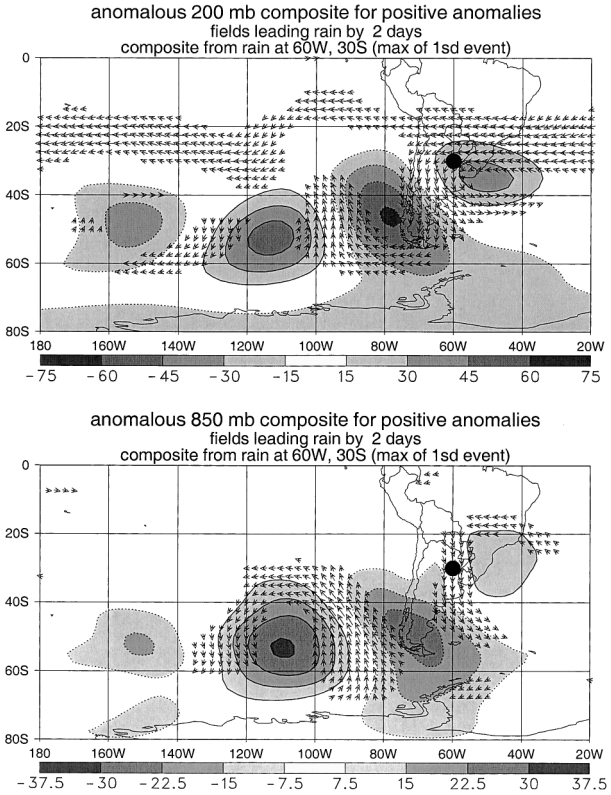

FIG. 7. (a) Composite anomalous 200-mb vector winds and heights that lead the 1 std dev rainfall event at 30°S, 60°W (dark circle) by 2 days. For each temporal excursion of rainfall above 1 std dev, only the maximum rain event is used to composite. Dotted curves indicate negative anomalies. (b) As in (a), except at 850 mb.

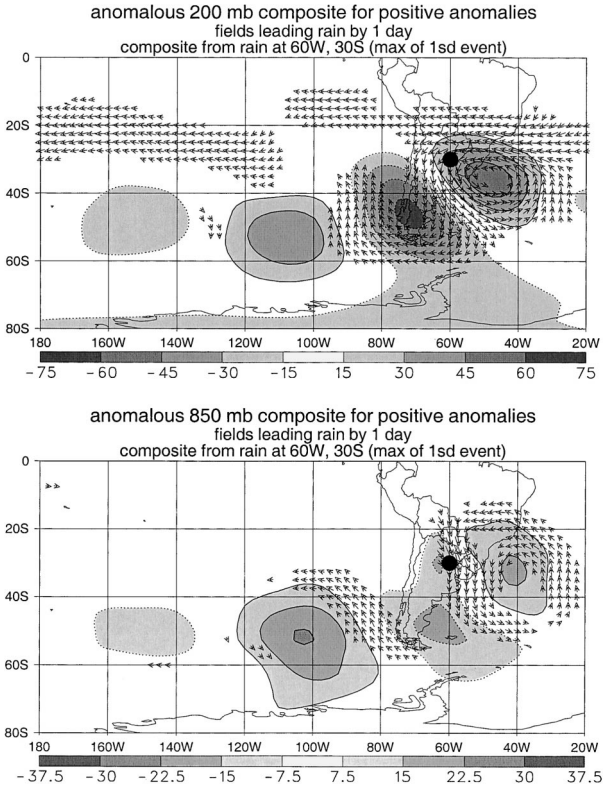

FIG. 8. As in Fig. 7, except the fields lead the rain event by 1 day.

at 20°S, 45°W. This grid point is along the axis of minimum DJF OLR associated with the SACZ and within the area where variance with periods less than 90 days is at a maximum (e.g., Liebmann et al. 1999).

Figures 11–13 show 200- and 850-mb heights and winds from 2 days before the day of the rain maximum to the day of the maximum in an event of at least one standard deviation rainfall anomaly at 20°S, 45°W. The circulation patterns leading up to a rainfall event near the jet and the SACZ, especially at upper levels, are both suggestive of midlatitude wave trains that turn northward as they cross the tip of South America. Overall, the SACZ pattern is weaker than that leading to rainfall associated with the jet, implying that in addition to the dominant wave train observed prior to rainfall in the SACZ, there are also other, less coherent patterns that produce rainfall there compared to in the jet area.

An important difference in the wave trains that ultimately strengthen the jet or result in rainfall in the SACZ, however, is that the upper-level patterns are quite close to being out of phase with each other. For example, 2 days prior to the rain maximum (Fig. 11 versus Fig. 7) the 200-mb anomalies are of similar magnitude near 50°S, 110°W, and 35°S, 50°W, although the anomalies near the tip of South America are centered on opposite sides of the mountains. One day before the rain maximum (Fig. 12 versus Fig. 8), the pattern associated with the jet has substantially higher amplitude; yet importantly, the winds in the vicinity of the jet, even at low levels, are in nearly opposite directions. On the day of rain maximum (Fig. 13 versus Fig. 9), the upper-level wave train associated with the SACZ has nearly disintegrated, but the center east of the jet point and south of the SACZ point remains strong. At 850 mb (Fig. 13b), the low centered slightly south of the SACZ base point continues to be associated with southerly winds in the vicinity of the jet, indicative of a weak jet. The low is in a similar position to the high shown in Fig. 9b, which is consistent with a geostrophic strengthening of the jet. Thus a simple hypothesis of an out-of-phase relationship between simultaneous rainfall anomalies downstream of the jet and in the SACZ is that the location of the rainfall anomaly depends on the phase of the wave as it approaches South America.

The base points from which height anomalies were composited are near the centers of the ''dipole'' observed by Nogués-Paegle and Mo (1997). Thus, the present results are consistent with precipitation in one center of the dipole being enhanced while the other is weak. On the other hand, Nogués-Paegle and Mo determined the dipole to have a half period near 10 days. Thus, the time scale for the lag between rainfall downstream of

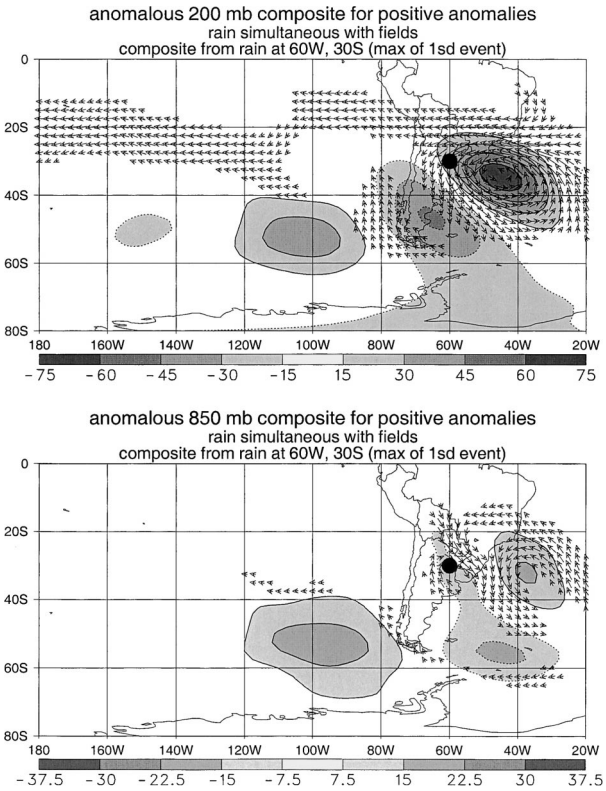

FIG. 9. As in Fig. 7, except the fields are simultaneous with the rain event.

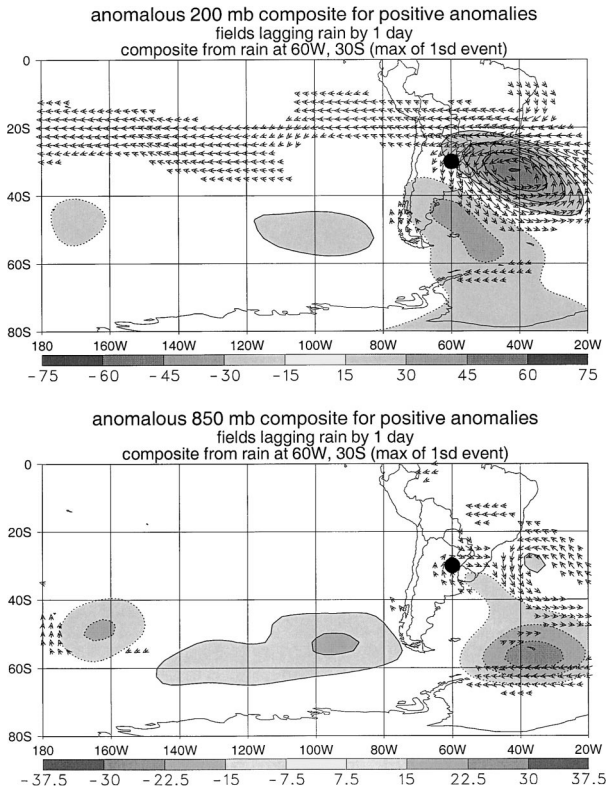

FIG. 10. As in Fig. 7, except the fields lag the rain event by 1 day.

the jet and in the SACZ is determined not by that of an individual synoptic wave to propagate between the two centers of activity, but rather by the intraseasonal variation of the dipole.

3) ASSOCIATIONS WITH THE MADDEN–JULIAN OSCILLATION

The MJO has the most important tropical influence on the global-scale circulation on intraseasonal time scales. Its signal features convection that forms over the Indian Ocean and then propagates eastward at about 5 m s^{-1} until it approaches the date line (e.g., Madden and Julian 1994), where its amplitude diminishes. The convective signal (e.g., in OLR) exhibits a broad spectral peak at planetary spatial scales at an intraseasonal time scale of 30–70 days (Salby and Hendon 1994; Wheeler and Kiladis 1999), although the dynamical signal is narrower in frequency. Thus the signal of the MJO readily lends itself to isolation through space–time filtering.

To capture variability associated with the MJO, daily OLR fields from 1979 to 2000 are filtered to include the zonal mean and eastward-propagating wavenumbers 1–9, and periods from 30–96 days (e.g., Wheeler and Kiladis 1999). From these filtered fields, an index is defined as the time series at 10°S, 110°E, hereafter referred to as the MJO index, which is the point of maximum filtered DJF variance. Maximum convective activity over that region occurs when the index is at a minimum.

Segments of the MJO time series are then composited relative to daily rainfall events that exceed one standard deviation above the DJF daily mean downstream of the jet at 30°S, 60°W (Fig. 14a). The base rainfall indices are the same as those used to produce Figs. 7–11, except that in this case all one standard deviation occurrences are included (rather than only the maximum day per excursion above the threshold) to increase the contribution to the composite by the largest sustained events. Thus, from this figure, one can determine whether there is a preference for rainfall anomalies to occur during a certain phase of the MJO.

The statistical relevance of Fig. 14a is estimated by randomly selecting from the MJO index the number of events (151) that went into the composite, averaging them, and recording the absolute value of that average. This procedure is repeated 999 times, and the value that is equaled or exceeded by 5% of the numbers is considered as the 95% significance level.

Figure 14a reveals several days with statistically relevant amplitudes of the MJO index relative to rainfall events downstream of the LLJ. There is a slight preference for rainfall events to follow the MJO convective

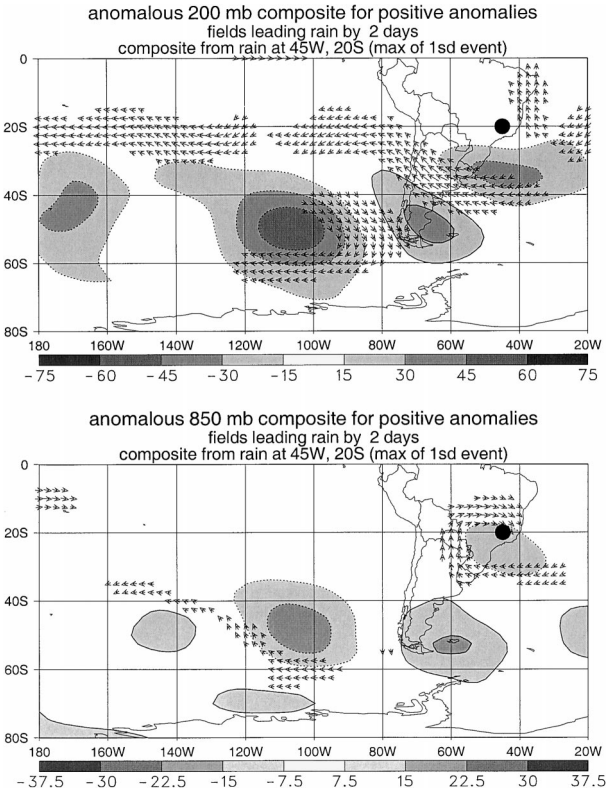

FIG. 11. As in Fig. 7, except the base rainfall grid point is at 20°S, 45°W.

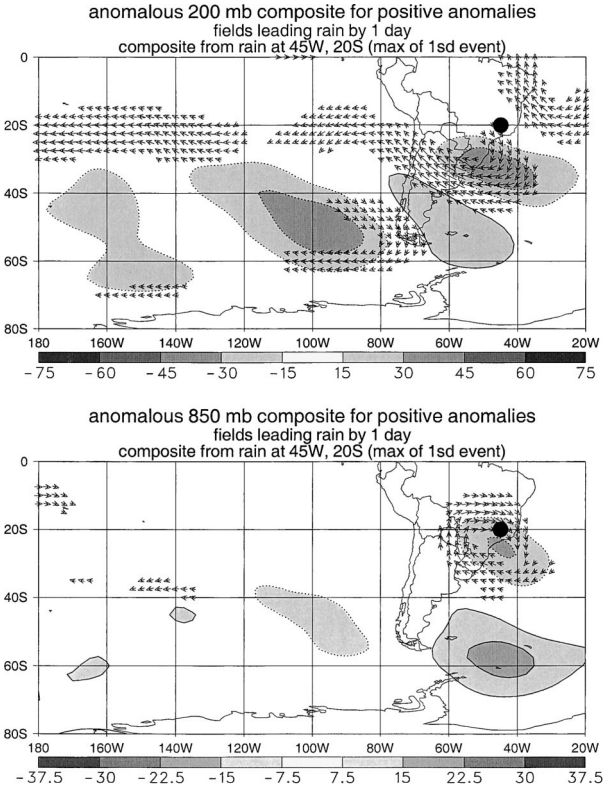

FIG. 12. As in Fig. 11, except the fields lead the rain event by 1 day.

maximum by 2 days, while suppressed convection in the MJO region precedes rainfall by 26 days.

Similar composites in the vicinity of the SACZ (Fig. 14b) show substantial variation of phase and amplitude of the composite signal at different grid points compared to the similarity of composites from different points downstream of the jet. At the climatological center of the SACZ (20°S, 45°W; thin curve), there is a preference for rainfall enhancement 26 days prior to the MJO index minimum (enhanced convection) and some evidence (not deemed statistically significant) of enhancement around 4 days after the MJO index maximum (suppressed convection). These relationships between rainfall events and MJO activity are also evident to the southwest (22.5°S, 47.5°W; thick curve), although there are phase shifts. At this point, however, there is also a preference for rainfall events to occur 26 days after the index minimum.

Figures 14a and 14b are complementary to each other in that together they confirm the existence of a dipole in precipitation (e.g., Nogués-Paegle and Mo 1997) associated with the MJO between rainfall downstream of the jet and slightly southwest of the mean position of the SACZ. For example, increased precipitation in both regions is associated with opposite MJO phases at about the same lag. This out-of-phase relationship is consistent with the seesaw pattern identified by Nogués-Paegle and Mo (1997), except that they found a half period of 10 days, while these figures indicate a half period closer to 20 days. This discrepancy affirms that the dipole is active on a variety of intraseasonal time scales.

Lead and lag regressions onto the MJO index are computed to examine the structure of precipitation, OLR, and circulation anomalies associated with the particular phases of the MJO that appear to be relevant to rainfall in the areas of present interest. Figure 14 shows that days around +26, +2, and −26 of the MJO cycle appear to be key in describing rainfall variations in the areas of interest. While day +2 is close to the peak of MJO convection at the index point, day +26 is associated with the decaying MJO event that was strongest at day 0, while day −26 is associated with the end of the previous event. Similar rainfall conditions occur over South America in the vicinity of the dipole for both the day −26 and day +26 regressions (not shown), consistent with the time scale for the MJO. Since it is physically more realistic to think of the MJO phase described by positive lags (i.e., following the main peak in the MJO rather than during the decay of the previous event), the analysis will focus on days +2 and +26.

Figure 15 shows the regressions of both rainfall and OLR anomalies onto the index 2 (Fig. 15a) and 26 (Fig. 15b) days after the peak of MJO convective activity as defined by the index. The statistical significance of these

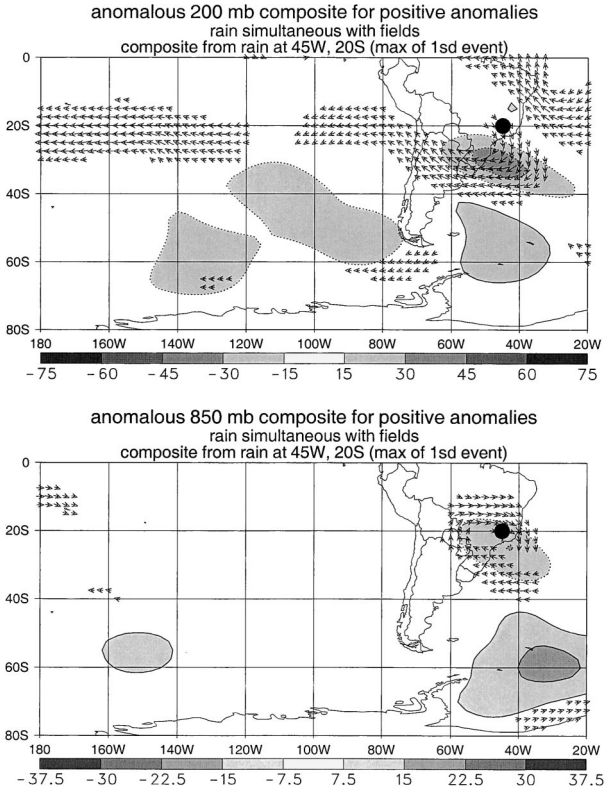

FIG. 13. As in Fig. 11, except the fields are simultaneous with the rain event.

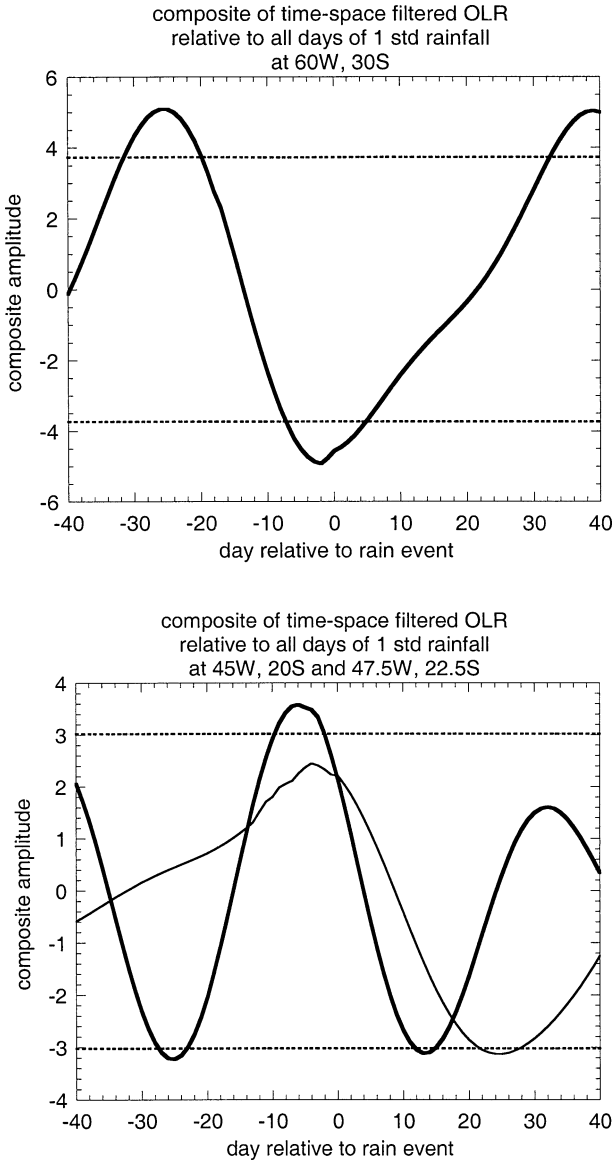

FIG. 14. (a) Composite of time–space-filtered MJO index (see text) at 10°S, 110°E relative to 1 std dev rainfall anomalies at (a) 30°S, 60°W and (b) both 20°S, 45°W (thin curve) and 22.5°S, 47.5°W (thick curve). Dotted lines represent the average of those randomizations whose absolute value is at or above the 95th percentile, from a total of 1000 randomizations. In (b), the statistical significance is estimated for the point at 22.5°S, 47.5°W, although it is quite similar to that at 20°S, 45°W.

fields has been determined by taking into account the autocorrelations of both the MJO index and the precipitation and OLR by the methodology described in Livezey and Chen (1983). At day +2, the centers of maxima and minima of the precipitation and OLR fields are locally significant at better than the 95% level, while at day +26 the OLR field passes this test, although the area covered is reduced. Both maps, except for precipitation at day +26, pass the field significance test, so for clarity we show the entire fields at each lag without regard to significance.

On the other hand, at day +26 (Fig. 15b), an approximate opposite condition exists, with positive rainfall anomalies in the vicinity of the SACZ and negative anomalies to the southwest, downstream of the LLJ.

The differences between precipitation and OLR anomalies in Figs. 15a and 15b are noteworthy. In both, OLR anomalies of the expected sign are in the maximum of climatological SACZ activity, while rainfall anomalies are strongest on the southern edge of mean SACZ activity. On the other hand, downstream of the jet, OLR anomalies are not evident in association with those in rainfall. As is known, OLR is not a good proxy for precipitation in the subtropics, and this may explain why the center of subtropical variability is substantially weaker than the center that describes the SACZ in the EOF analysis shown by Nogués-Paegle and Mo (1997, their Fig. 3).

Figure 16a shows the global day +2 circulation at 200 hPa, when convection over the Maritime Continent is nearly at its strongest. All patterns in this and the following figure are highly field significant (except rainfall at day +26). The large-scale pattern is consistent with many previous studies of the MJO (e.g., Knutson and Weickmann 1987; Kiladis and Weickmann 1992; Hendon and Salby 1994), and is somewhat similar to

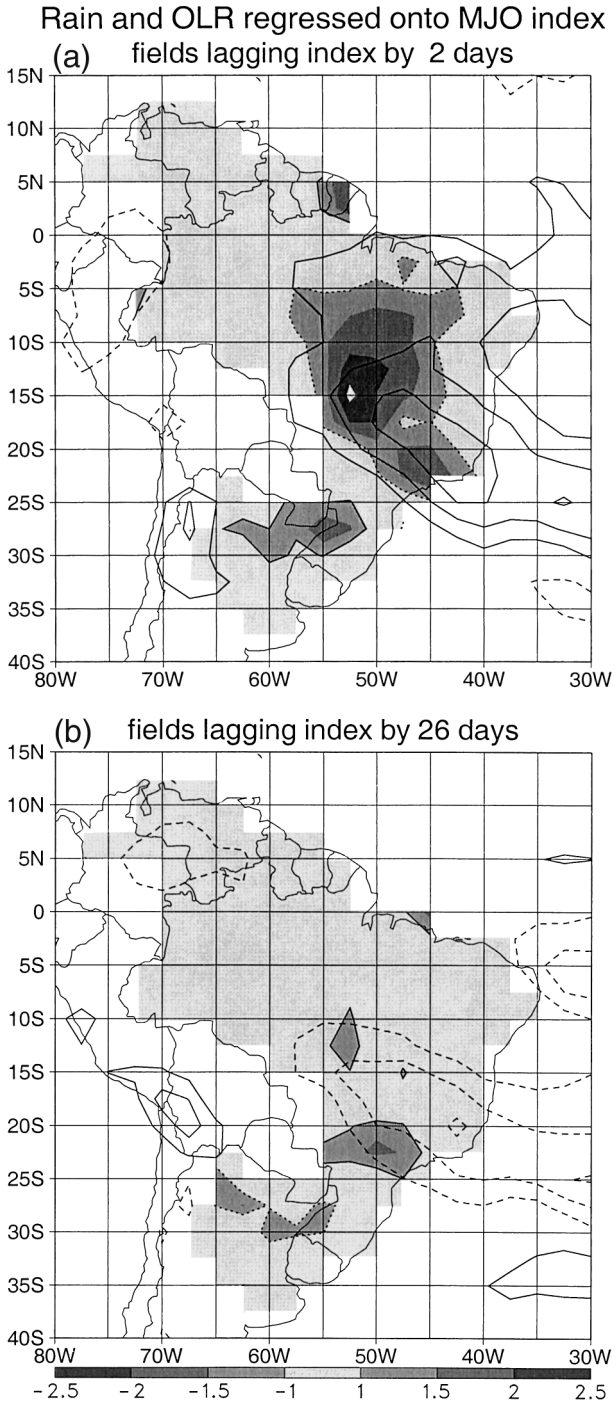

FIG. 15. Regressions of DJF precipitation and OLR onto filtered (see description in text) OLR at 10°S, 110°E for (a) 2 days and (b) 26 days after the minimum at the grid point (maximum convection). Regressions are scaled to a 40 W m^{-2} anomaly of the index. Solid contours surround positive precipitation anomalies, and dotted contours surround negative anomalies. OLR anomalies exceeding ±4.0 W m^{-2} are shaded. Solid (dashed) contours indicate positive (negative) OLR anomalies.

the OLR pattern found over South America by Carvalho et al. (2004) using an EOF-based definition of the MJO. A cyclonic circulation is centered near the east coast of southern Argentina, an anticyclonic circulation is northeast of the positive rainfall anomaly at 30°S, 60°W, and 200-mb zonal easterlies cross South America at about 20°S.

At 850 mb (Fig. 17a), northwesterly anomalies indicate a strengthened low-level jet. A comparison between the circulation composite patterns based on the LLJ point (Figs. 9a,b) and those depicted by the regression maps based on the MJO index (Figs. 16a and 17a) reveals strong similarities over South America. Furthermore, the upper-level cyclonic anomaly and the low-level anticyclonic anomaly, both associated with enhanced precipitation downstream of the LLJ, seem to be the features most influenced by the MJO activity.

At day +26 (Fig. 16b), when the SACZ is active, the MJO-related convective anomalies are approximately opposite to those at day +2. Over South America, an upper-level zonally elongated trough extends over the subtropics, while the 850-mb pattern (Fig. 17b) reveals a cyclonic circulation centered west of the SACZ point. Again, MJO-related circulation patterns are similar to those depicted by the composites for the SACZ (Fig. 13), although there are some discrepancies, particularly in lower levels.

4. Summary and discussion

The purpose of the research presented here is to identify rainfall and large-scale circulation anomalies associated with variations in the South American low-level jet. A comparison is also made between these and anomalies associated with rainfall variations in the vicinity of the SACZ.

Composites of rainfall associated with strong jets reveal an approximate doubling of the quantities one would expect from climatology. The anomaly first appears in the south of the domain, in central Argentina, and moves northward with time. The count of extreme precipitation events follows the same pattern. The extreme event composite also shows a decrease of extremes associated with the jet in a zonal strip just south of the equator and an increase in Venezuela. An expected dearth of extremes is evident when the jet is weak.

Winds and circulation in the vicinity of the jet are then composited based on rainfall at 30°S, 60°W, which is near the maximum rainfall anomaly associated with the jet as defined in this study. At 20°S, the composite jet is distinct, with a wind maximum near 850 mb. Farther south, however, while there is a local low-level maximum, composite winds generally increase with height to about 200 mb, suggestive of a synoptic baroclinic wave forcing the jet. This is confirmed by composites of heights, temperature, and large-scale wind anomalies, which suggest a wave train that originates

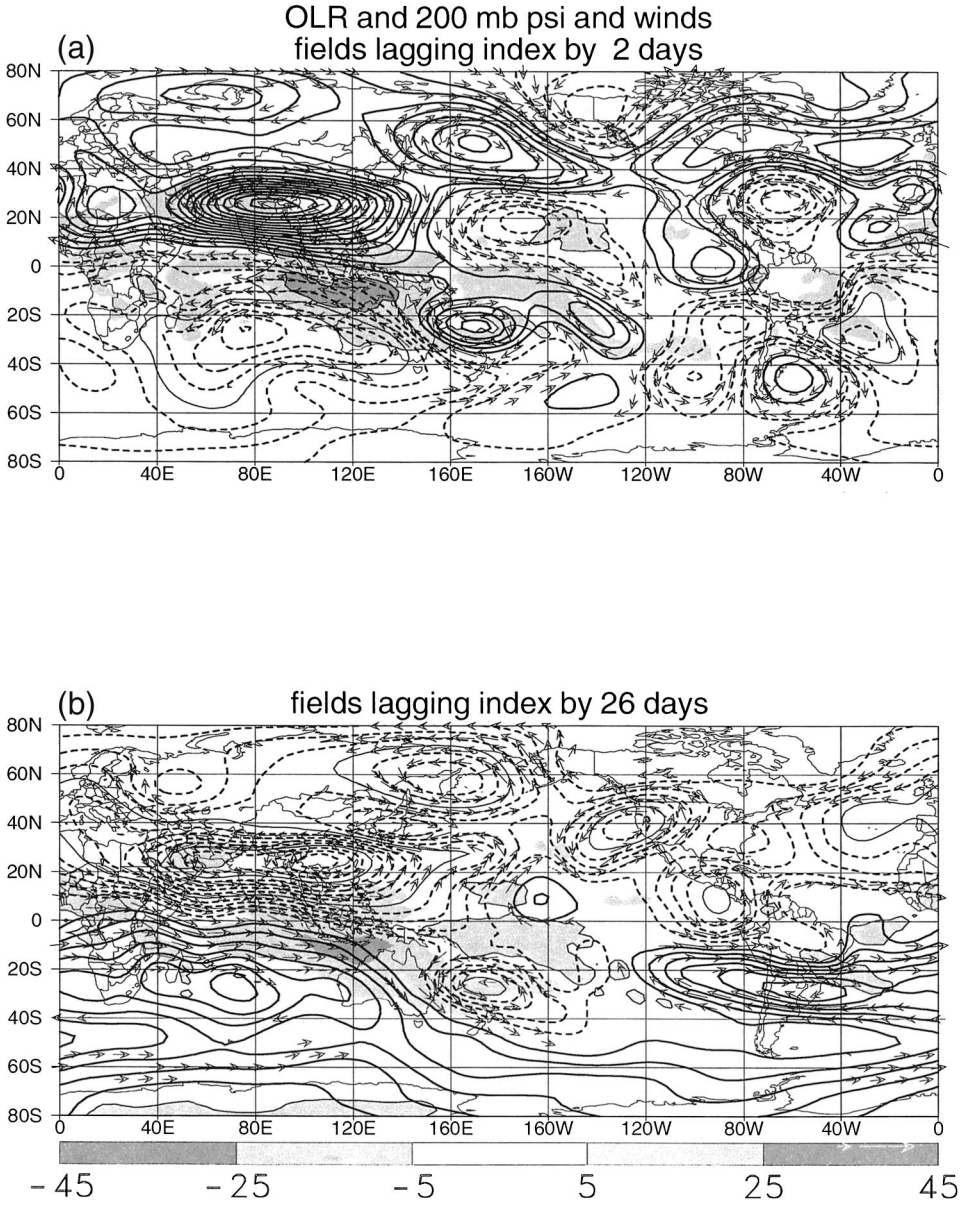

FIG. 16. As in Fig. 15, except for regressions of OLR (shaded; anomalies in W m^{-2}), 200-mb vector winds, and 200-mb streamfunction (contoured). Vector winds are plotted when speed anomalies exceed 2.0 m s^{-1}. Streamfunction contours start at $\pm 10 \times 10^5$ m^2 s^{-1}, with negative contours dashed.

in the midlatitude Pacific and turns equatorward as it crosses the Andes.

Lead and lag composites of circulation for rainfall anomalies associated with the jet are compared to those based on rain in the SACZ. There are some similar features between the two composites, but the anomalies are of opposite sign, suggesting that on a daily time scale, a preference for rain in the SACZ should coincide with a weak jet and dry conditions downstream of it, and vice versa. Dipole precipitation anomalies of opposite sign in the locations investigated here have been noted in many previous studies on several time scales. However, there is a preference for synoptic-scale waves approaching the Andes to propagate more zonally, so that the disturbances moving northward appear to require a certain basic state that leads to the tilting associated with equatorward propagation.

An index describing the MJO is composited relative to one standard deviation rainfall events. The amplitude is judged to be statistically significant both for events downstream of the jet and slightly south of the center of the SACZ. Rainfall events downstream of the jet are slightly more likely to occur 2 days after the peak in convection as determined by the MJO index, while

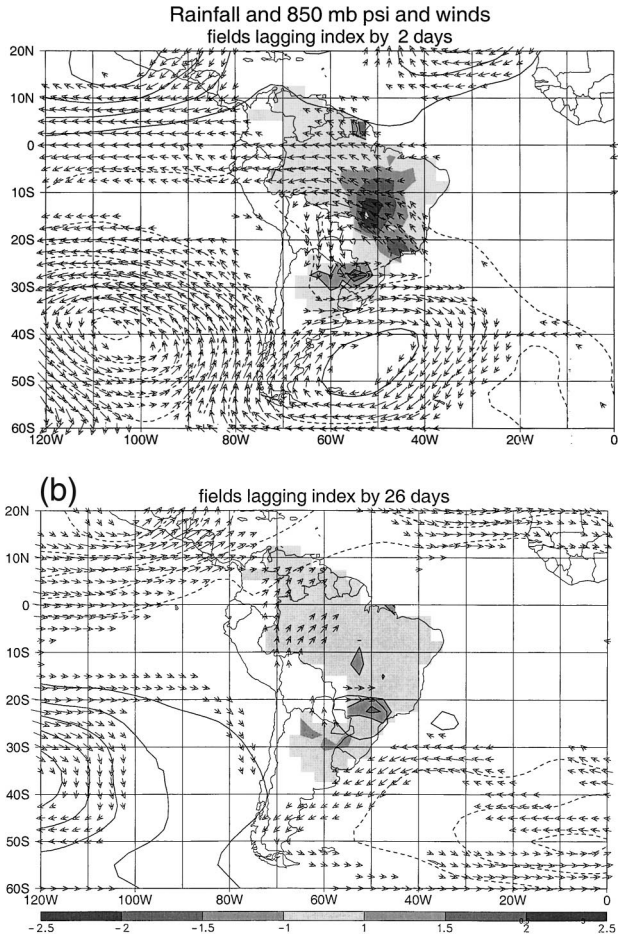

FIG. 17. As in Fig. 15, except for precipitation (shaded; anomalies in mm day^{-1}), vector winds, and streamfunction at 850 mb. Vector winds are plotted when speed anomalies exceed 0.5 m s^{-1}. Streamfunction contours start at $\pm 4 \times 10^5$ m^2 s^{-1}, with negative contours dashed.

SACZ events show a slight preference to occur 26 days after the index peak. These phases of the MJO are approximate opposites of each other.

In the SACZ, OLR anomalies represent those in precipitation in a large-scale sense. In the subtropics, however, OLR is clearly inadequate, reiterating the need for a dense network of grand-based observations.

While statistically relevant, the preferences for rainfall events downstream of the jet and in the SACZ to occur during different phases of the MJO represent a small change in probability. Whether this change in probability is due to changes in the structure and propagation of the synoptic waves from the Pacific into South America, or whether the slowly varying background flow in the vicinity of South America is influenced by the MJO and results in different propagation characteristics, is not yet understood and will be a topic of future research.

Acknowledgments. The following agencies provided rainfall data that were used in this study: Agência Nacional de Energia Elétrica of Brazil, Servicio Meteorologico Nacional of Argentina, C.T.M. Salto Grande, U.T.E. Uruguay, Servicio Meteorologico Nacional of Uruguay, Ministerio del Ambiente y los Recursos Naturales of Venezuela, FUNCEME of the state of Ceará, Brazil, SIMEPAR of the state of Paraná, Brazil, DAEE of the state of São Paulo, Brazil, and the national weather services of Surinam and French Guiana. We also wish to thank the Inter-American Institute for Global Change Research (IAI-CRN-055) for providing funds to allow collaboration between the Argentinean and U.S. investigators and the CLIVAR Pan American Climate Studies Program (GC01-351 and GC03-011).

REFERENCES

Ambrizzi, T., and B. J. Hoskins, 1997: Stationary Rossby-wave propagation in a baroclinic atmosphere. *Quart. J. Roy. Meteor. Soc.*, **123,** 919–928.

Berbery, E. H., J. Nogués-Paegle, and J. Horel, 1992: Wavelike Southern Hemisphere extratropical teleconnections. *J. Atmos. Sci.,* **49,** 155–177.

Berri, G. J., and J. Inzunza B., 1993: The effect of the low-level jet on the poleward water vapour transport in the central region of South America. *Atmos. Environ.*, **27A,** 335–341.

Bonner, W. D., 1968: Climatology of the low level jet. *Mon. Wea. Rev.,* **96,** 833–850.

Brooks, C. E. P., and N. Carruthers, 1953: *Handbook of Statistical Methods in Meteorology.* Her Majesty's Stationary Office, 412 pp.

Campetella, C., and C. Vera, 2002: The influence of the Andes Mountains on the South American low-level flow. *Geophys. Res. Lett.*, **29,** 1826, doi:10.1029/2002GL015451.

Carvalho, L. M. V., C. Jones, and B. Liebmann, 2004: The South Atlantic convergence zone: Intensity, form, persistence, and relationships with intraseasonal to interannual activity and extreme rainfall. *J. Climate*, **17,** 88–108.

Casarin, D. P., and V. E. Kousky, 1986: Anomalias de precipitacão no sul do Brasil e variacoes na circulacão atmosferica. *Rev. Bras. Meteor.*, **1,** 83–90.

Douglas, M. W., M. Nicolini, and C. Saulo, 1998: Observational evidences of a low level jet east of the Andes during January–March 1998. *Meteorologica,* **23,** 63–72.

——, M. Peña, and W. R. Villarpando, 2000: Special observations of the low-level flow over eastern Bolivia during the 1999 Atmospheric Mesoscale Campaign. Preprints, *Sixth Int. Conf. on Southern Hemisphere Meteorology and Oceanography*, Santiago, Chile, Amer. Meteor. Soc., 157–158.

Ferranti, L., T. N. Palmer, F. Molteni, and E. Klinker, 1990: Tropical–extratropical interaction associated with the 30–60 day oscillation and its impact on medium and extended range prediction. *J. Atmos. Sci.,* **47,** 2177–2199.

Figueroa, S. N., P. Satyamurty, and P. L. da Silva Dias, 1995: Simulations of the summer circulation over the South American region with an eta coordinate model. *J. Atmos. Sci.*, **52**, 1573–1584.

Garreaud, R. D., and J. M. Wallace, 1998: Summertime incursions of midlatitude air into subtropical and tropical South America. *Mon. Wea. Rev.*, **126,** 2713–2733.

Hendon, H. H., and M. L. Salby, 1994: The life cycle of the Madden–Julian oscillation. *J. Atmos. Sci.,* **51,** 2225–2237.

Herdies, D. L., A. da Silva, M. A. F. Silva Dias, and R. Nieto Ferreira, 2002: Moisture budget of the bimodal pattern of the summer circulation over South America. *J. Geophys. Res.,* **107,** 8075, doi:10.1029/2001JD000997.

Jones, C., and L. M. V. Carvalho, 2002: Active and break phases in the South American monsoon system. *J. Climate,* **15,** 905–914.

——, ——, R. W. Higgins, D. E. Waliser, and J.-K. Schemm, 2004: A statistical forecast model of tropical intraseasonal convective anomalies. *J. Climate,* **17,** 2078–2095.

Kalnay, E., and Coauthors, 1996: The NCEP/NCAR 40-Year Reanalysis Project. *Bull. Amer. Meteor. Soc.,* **77,** 437–471.

Kiladis, G. N., and K. M. Weickmann, 1992: Circulation anomalies associated with tropical convection during northern winter. *Mon. Wea. Rev.,* **120,** 1900–1923.

Knutson, T. R., and K. M. Weickmann, 1987: 30–60 day atmospheric oscillations: Composite life cycles of convection and circulation anomalies. *Mon. Wea. Rev.,* **115,** 1407–1436.

Kodama, Y.-M., 1993: Large-scale common features of sub-tropical convergence zones (the Bai-u frontal zone, the SPCZ, and the SACZ). Part II: Conditions of the circulations for generating the STCZs. *J. Meteor. Soc. Japan,* **71,** 581–610.

Lenters, J. D., and K. H. Cook, 1999: Summertime precipitation variability over South America: Role of the large-scale circulation. *Mon. Wea. Rev.,* **127,** 409–431.

Li, Z. X., and H. Le Treut, 1999: Transient behavior of the meridional moisture transport across South America and its relation to atmospheric circulation patterns. *Geophys. Res. Lett.,* **26,** 1409–1412.

Liebmann, B., G. N. Kiladis, J. A. Marengo, T. Ambrizzi, and J. D. Glick, 1999: Submonthly convective variability over South America and the South Atlantic convergence zone. *J. Climate,* **12,** 1877–1891.

——, C. Jones, and L. M. V. de Carvalho, 2001: Interannual variability of daily extreme precipitation events in the state of São Paulo, Brazil. *J. Climate,* **14,** 208–218.

Livezey, R. E., and W. Y. Chen, 1983: Statistical field significance and its determination by Monte Carlo techniques. *Mon. Wea. Rev.,* **111,** 46–59.

Madden, R. A., and P. R. Julian, 1994: Observations of the 40–50-day oscillation—A review. *Mon. Wea. Rev.,* **122,** 814–837.

Marengo, J. A., M. W. Douglas, and P. L. Silva Dias, 2002: The South American low-level jet east of the Andes during the 1999 LBA-TRMM and LBA-WET AMC campaign. *J. Geophys. Res.,* **107,** 8079, doi:10.1029/2001JD001188.

Marton, E., and P. L. Silva Dias, 2001: Variabilidade intrasazonal na Zona de Convergência do Atlântico Sul. *IX Congreso Latinoamericano e lberico de Meteorología y VIII Congreso Argentino de Meteorología: La Meteorología y el Medio Ambiente en el Siglo XXI,* Buenos Aires, Argentina, ANAIS DIGITAIS, CD-ROM, 5.A.25–179.

Mo, K. C., and R. W. Higgins, 1996: Large-scale atmospheric moisture transport as evaluated in the NCEP/NCAR and the NASA/DAO reanalyses. *J. Climate,* **9,** 1531–1545.

Nicolini, M., and A. C. Saulo, 2000: ETA characterization of the 1997–98 warm season Chaco jet cases. Preprints, *Sixth Int. Conf. on Southern Hemisphere Meteorology and Oceanography,* Santiago, Chile, Amer. Meteor. Soc., 330–331.

Nieto Ferreira, R., T. M. Rickenbach, D. L. Herdies, and L. M. V. Carvalho, 2003: Variability of South American convective cloud systems and tropospheric circulation during January–March 1998 and 1999. *Mon. Wea. Rev.*, **131,** 961–973.

Nogués-Paegle, J., and K. C. Mo, 1997: Alternating wet and dry conditions over South America during summer. *Mon. Wea. Rev.,* **125,** 279–291.

Paegle, J., 2000: American low-level jets in observation and theory: The ALLS project. Preprints, *Sixth Int. Conf. on Southern Hemisphere Meteorology and Oceanography,* Santiago, Chile, Amer. Meteor. Soc., 161–162.

Paegle, J. N., L. A. Byerle, and K. C. Mo, 2000: Intraseasonal modulation of South American summer precipitation. *Mon. Wea. Rev.,* **128,** 837–850.

Salby, M. L., and H. H. Hendon, 1994: Intraseasonal behavior of clouds, temperature, and motion in the Tropics. *J. Atmos. Sci.,* **51,** 2207–2224.

Salio, P., M. Nicolini, and A. C. Saulo, 2002: Chaco low-level jet events characterization during the austral summer season. *J. Geophys. Res.,* **107,** 4816, doi:10.1029/2001JD001315.

Saulo, A. C., and M. Nicolini, 2000: The atmospheric conditions preceding the occurrence of a strong low level jets east of the Andes during January 1998. Preprints, *Sixth Int. Conf. on Southern Hemisphere Meteorology and Oceanography,* Santiago, Chile, Amer. Meteor. Soc., 336–337.

Silva Dias, P. L., 2000: The role of latent heat release in the dynamics of the LLJ's along the Andes. Preprints, *Sixth Int. Conf. on Southern Hemisphere Meteorology and Oceanography,* Santiago, Chile, Amer. Meteor. Soc., 163–164.

Stensrud, D. J., 1996: Importance of low-level jets to climate: A review. *J. Climate,* **9,** 1698–1711.

Sugahara, S., R. P. da Rocha, and M. L. Rodrigues, 1994: Atmospheric conditions associated with the South America low level jet (in Portuguese). *Proc. Eighth Brazilian Congress of Meteorology,* Vol. 2, Belo Horizonte, Brazil, Brazilian Meteorological Society, 573–577.

Vera, C., P. K. Vigliarolo, and E. H. Berbery, 2002: Cold season synoptic-scale waves over subtropical South America. *Mon. Wea. Rev.,* **130,** 684–699.

Wheeler, M., and G. N. Kiladis, 1999: Convectively coupled equatorial waves: Analysis of clouds and temperature in the wavenumber–frequency domain. *J. Atmos. Sci.,* **56,** 374–399.